Elastic constants of layers in isotropic laminates

Paul R. Heyliger
Department of Civil Engineering, Colorado State University, Fort Collins, Colorado 80523

Hassel Ledbetter
Los Alamos National Laboratory (E536), Los Alamos, New Mexico 87545

Sudook Kim
Materials Science and Engineering Laboratory, National Institute of Standards and Technology, Boulder, Colorado 80305

Ivar Reimanis
Metallurgical and Materials Engineering Department, Colorado School of Mines, Golden, Colorado 80401

(Received 21 June 2002; revised 25 November 2002; accepted 25 August 2003)

The individual laminae elastic constants in multilayer laminates composed of dissimilar isotropic layers were determined using ultrasonic-resonance spectroscopy and the linear theory of elasticity. Ultrasonic resonance allows one to measure the free-vibration response spectrum of a traction-free solid under periodic vibration. These frequencies depend on pointwise density, laminate dimensions, layer thickness, and layer elastic constants. Given a material with known mass but unknown constitution, this method allows one to extract the elastic constants and density of the constituent layers. This is accomplished by measuring the frequencies and then minimizing the differences between these and those calculated using the theory of elasticity for layered media to select the constants that best replicate the frequency-response spectrum. This approach is applied to a three-layer, unsymmetric laminate of W_pCu, and very good agreement is found with the elastic constants of the two constituent materials. © *2003 Acoustical Society of America.*
[DOI: 10.1121/1.1618754]

Pages: 2618–2625

PACS numbers: 43.20.Ks, 43.40.Dx [YHB]

I. INTRODUCTION

Determining the elastic constants of materials with unknown constitution is a much-studied problem in science and engineering, and there are numerous methods available for solving it. One method that is particularly robust is ultrasonic-resonance spectroscopy (URS), in which the free-vibration response spectrum of the solid is used in combination with the theoretical values of frequencies for objects with known density, geometry, and elastic constants.[1–6] Numerous applications of this method, along with descriptions of the experimental system, measurements, and theoretical analysis, are given in Migliori and Sarrao.[6] The theoretical predictions are based on the Ritz method, in which the solution of the weak form of the equations of periodic motion is sought as given in Hamilton's principle, where the displacements are given in a finite series in terms of the spatial coordinates of the specimen geometry. Excellent accuracy can be obtained using this approach.

To date, most applications of URS for the determination of elastic constants have been for homogeneous media. Consistent with these applications, the computational algorithms developed for this purpose have without exception used basis functions for the displacement components that have been continuous with continuous derivatives (such as the Legendre polynomials used for parallelepipeds by Demarest[2] and power series as used in the more general method developed by Visscher and colleagues[7]). This is a valid and useful approach for homogeneous media, but special care must be taken when considering dissimilar media. At an interface between two materials that differ in elastic properties, the transverse shear stresses are continuous across the interface but there is a jump in shear modulus. Hence, there is a discontinuity in the through-thickness displacement gradient that cannot be represented using functions with C^1 continuity (i.e., functions such as power series, which possess continuous first derivatives over the specimen domain).

Recently, we developed a method to account for the through-thickness behavior of laminated elastic and piezoelectric media.[8] This method is based on a discrete-layer approximation to the weak form of the equations of motion, in which we split the through-thickness and in-plane dependence of the approximation functions in the Ritz method. Similar approaches have been used in related problems by Pauley and Dong[9] for wave propagation in laminated piezoelectric media, and a generalized discrete-layer approach for elastic laminates by Reddy.[10] With this model in hand, our present objective is to evaluate the elastic constants and densities of layered parallelepipeds where only the edge dimensions, layer thicknesses, total mass, and free-vibration-response spectra are given. To our knowledge, this is the first application of URS to dissimilar composites of this type, and it results in a method where, rather than separating the individual constituents of the composite, we can consider the component as a whole.

II. MATERIAL

Three-layer W_p/Cu laminates were fabricated by a powder-metallurgy approach in which powders of specific compositions were mixed, layered, and then densified in a hot press. High-purity (99.9) 1–5-μm-diameter copper

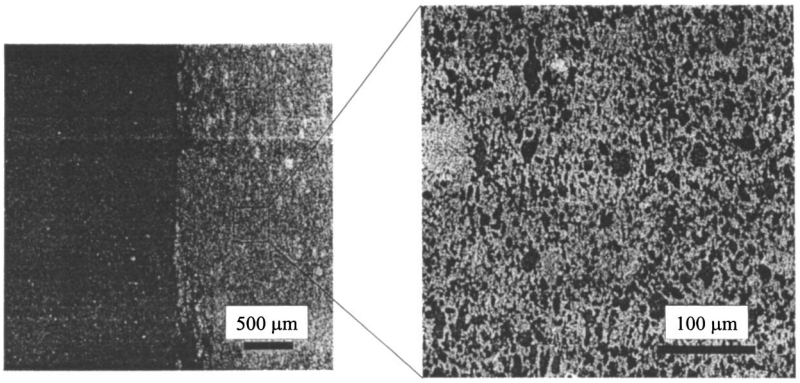

FIG. 1. Microstructure of the trilayer composite interface and the copper/tungsten composite.

powder[11] was mixed with high-purity (99.95) W powder with an average particle diameter of 1 μm.[12] Cu–W powders were made by mixing amounts of pure W and Cu that would lead to a 20 percent composite when fully dense, and milling in a polycarbonate bottle with four to five cleaned alumina balls for 24 h. The laminate was made by pouring first the Cu–W powder, then the pure Cu powder, and finally more Cu–W powder into a 25.4-mm-diameter graphite die. The inner walls of the die were coated with BN to prevent chemical reaction with carbon. After each powder type was poured, a clean steel punch was used for leveling. This resulted in a powder stack consisting of 20%W/0%W/20%W. The stacked powders were then sintered in a hot press under a vacuum of 1.33×10^{-2} Pa, a load of 40 MPa at 985 °C for 15 min. Cooling was accomplished with the load still applied at a rate of about 20 °C/min, until about 500 °C, at which point the rate slowed substantially. A dense trilayer sample consisting of 20%W/0%W/20%W resulted, with layer thicknesses of 1.50 mm/1.88 mm/1.66 mm, respectively.

The composite microstructure and the nature of the interface between layers is apparent in the scanning electron micrograph shown in Fig. 1. The light and dark contrasts represent the W and Cu, respectively. Consistent with the fact that Cu and W do not react and are mutually insoluble, observations in the scanning electron microscope (SEM) indicated that the interface between the 20% W and 0% W layers represents a discrete transition between these compositions, without the presence of a discernible interphase. (The SEM's resolution limit is approximately 0.1 μm). The interface plane does exhibit some roughness. Typically, the interface position varies by less than 100 μm over 2 mm.

Single-composition composites (20% W and pure Cu) were produced as described above to measure the elastic properties of the material in the outer layers. The hot-pressed trilayer composites were subsequently cut by diamond saw into specimens of dimensions $7.01\times7.84\times5.04$ mm, with the layers in the third dimension. Single-composition specimens were cut by electrodischarge machining to dimensions $10.0\times9.0\times8.0$ mm, with no layers.

III. THEORY

A. Geometry and boundary conditions

The rectangular parallelepiped described in the previous section is a special case of the general layered block assumed in our theoretical calculations. The parallelepiped is in general composed of an arbitrary number of elastic and isotropic layers. The parallelepiped has dimensions L_x, L_y, and L_z, and the z direction is perpendicular to each dissimilar-material interface. Each layer has constitutive equations that can be expressed as[13]

$$\sigma_{ij}=\lambda\,\delta_{ij}e_{kk}+2\mu e_{ij}\,. \tag{1}$$

Here, λ and μ are the Lamé parameters, δ_{ij} is the Kronecker delta, σ_{ij} are the components of stress, and e_{ij} are the components of infinitesimal strain. We also use the alternate form of the constitutive relation

$$\sigma_{ij}=C_{ijkl}e_{kl}\,, \tag{2}$$

where the C_{ijkl} are the components of the elastic-stiffness tensor, which can be expressed in terms of the two Lamé parameters. The strain-displacement relations are given by

$$e_{ij}=\frac{1}{2}\left(\frac{\partial u_i}{\partial x_j}+\frac{\partial u_j}{\partial x_i}\right). \tag{3}$$

Here, u_i represent the displacement components.

Hamilton's principle forms the basis for the weak form of the equations of motion[14]

$$\delta\int_{t_0}^{t}dt\int_V\left[\frac{1}{2}\rho\dot{u}_j\dot{u}_j-U_o(e_{kl})\right]dV+\int_{t_0}^{t}dt\int_S\overline{T}_k\delta u_k\,dS=0. \tag{4}$$

Here, t is time, V and S are the volume and surface occupied by and bounding the solid, $\overline{T}$ are the specified surface tractions, δ is the variational operator, the overdot superscript represents differentiation with respect to time, and U_o represents the strain-energy density, given for a linear elastic material as

$$U=\tfrac{1}{2}C_{ijkl}e_{ij}e_{kl}\,. \tag{5}$$

The weak form of the governing equations, as well as the governing differential equations themselves, can be found by substituting the above relations into Hamilton's principle. Here, we use the usual contracted notation for the elastic stiffnesses C_{ijkl} by compressing the ij and kl indices into a single index ranging from 1 to 6, and maintaining the range of m from 1 to 3. For example, C_{1122} becomes C_{12}, and so on. In rectangular Cartesian coordinates, we set $x_1=x$, $x_2=y$, and $x_3=z$, with the displacements as $u_1=u(x,y,z)$, $u_2=v(x,y,z)$, and $u_3=w(x,y,z)$. The weak form can be expressed using this nomenclature as

$$\delta\int_{t_0}^{t} dt \int_V \Big[\rho(\dot{u}\,\delta\dot{u}+\dot{v}\,\delta\dot{v}+\dot{w}\,\delta\dot{w}) - \Big[C_{11}\frac{\partial u}{\partial x}\frac{\partial \delta u}{\partial x} + C_{12}\frac{\partial u}{\partial x}\frac{\partial \delta v}{\partial y} + C_{13}\frac{\partial u}{\partial x}\frac{\partial \delta w}{\partial z} + C_{12}\frac{\partial v}{\partial y}\frac{\partial \delta u}{\partial x} + C_{22}\frac{\partial v}{\partial y}\frac{\partial \delta v}{\partial y}$$
$$+ C_{23}\frac{\partial v}{\partial y}\frac{\partial \delta w}{\partial z} + C_{13}\frac{\partial w}{\partial z}\frac{\partial \delta u}{\partial x} + C_{23}\frac{\partial w}{\partial z}\frac{\partial \delta v}{\partial y} + C_{33}\frac{\partial w}{\partial z}\frac{\partial \delta w}{\partial z} C_{44}\left(\frac{\partial v}{\partial z}+\frac{\partial w}{\partial y}\right)\left(\frac{\partial \delta v}{\partial z}+\frac{\partial \delta w}{\partial y}\right)$$
$$+ C_{55}\left(\frac{\partial u}{\partial z}+\frac{\partial w}{\partial x}\right)\left(\frac{\partial \delta u}{\partial z}+\frac{\partial \delta w}{\partial x}\right) + C_{66}\left(\frac{\partial u}{\partial y}+\frac{\partial v}{\partial x}\right)\left(\frac{\partial \delta u}{\partial y}+\frac{\partial \delta v}{\partial x}\right)\Big]\Big] dV + \int_{t_0}^{t} dt \int_S \overline{T}_k \delta u_k \, dS = 0. \tag{6}$$

B. Discrete-layer approximation

In many past studies, approximations to the three displacements are generated in terms of the global (x,y,z) coordinates. In this study, the dependence of the displacements on the z coordinate is separated from the functions in x and y. This allows for global functions in x and y that result in a subsequent reduction of the size of the computational problem. Hence, approximations for the three displacement components are sought in the form[10]

$$u(x,y,z,t) = \sum_{i=1}^{m}\sum_{j=1}^{n} U_{ji}(t)\Psi_i^u(x,y)\overline{\Psi}_j^u(z),$$
$$v(x,y,z,t) = \sum_{i=1}^{m}\sum_{j=1}^{n} V_{ji}(t)\Psi_i^v(x,y)\overline{\Psi}_j^v(z), \tag{7}$$
$$w(x,y,z,t) = \sum_{i=1}^{m}\sum_{j=1}^{n} W_{ji}(t)\Psi_i^w(x,y)\overline{\Psi}_j^w(z).$$

Here, m and n are the respective number of in-plane and through-thickness terms used to approximate each variable. The approximations for each of the three field quantities are constructed in such a way as to separate the dependence in the planar coordinate variables from that in the coordinate variable perpendicular to the interface. The reason for this is that the change in the material properties forces a break in the gradients of the displacements across an interface. This can be seen easily by considering the case of shear stress at a dissimilar-material interface. Since the stress must be continuous across an interface but the shear modulus is different for two layers, the shear strain must be different. This implies that the slope of the displacement variables across the interface must be different, thus eliminating functions such as the commonly used power series[7] or Legendre polynomials.[3]

In the thickness direction, one-dimensional Lagrangian interpolation polynomials are used for $\overline{\Psi}_j(z)$. For the in-plane approximations, different types of approximations can be used for the two-dimensional functions $\Psi_j(x,y)$. We use power series for the problem of traction-free vibration. For a parallelepiped with n layers $(n-1)$ is the number of subdivisions through the parallelepiped thickness (typically taken equal to or greater than the number of layers in the parallelepiped), and Γ_{ji} is the value of component Γ at height j corresponding to the ith in-plane approximation function.[10]

Substituting these approximations into the weak form in Eq. (6), introducing the assumption of periodic motion, collecting the coefficients of the variations of the displacements, and placing the results in matrix form, we obtain the result

$$\rho\omega^2\begin{bmatrix}[M^{11}] & [0] & [0]\\ [0] & [M^{22}] & [0]\\ [0] & [0] & [M^{33}]\end{bmatrix}\begin{Bmatrix}\{u\}\\ \{v\}\\ \{w\}\end{Bmatrix}$$
$$-\begin{bmatrix}[K^{11}] & [K^{12}] & [K^{13}]\\ [K^{21}] & [K^{22}] & [K^{23}]\\ [K^{31}] & [K^{32}] & [K^{33}]\end{bmatrix}\begin{Bmatrix}\{u\}\\ \{v\}\\ \{w\}\end{Bmatrix} = \begin{Bmatrix}\{0\}\\ \{0\}\\ \{0\}\end{Bmatrix}. \tag{8}$$

The elements of these submatrices are themselves submatrices whose elements are determined by evaluating the preintegrated elastic stiffnesses through the thickness multiplied by the various shape functions or their derivatives as determined by the variational statement. If these submatrices, each of order $(n+1)$, are defined by the subscripts α and β,

TABLE I. Groupings of approximation functions.

Group	Displacement	x	y	z	Group	Displacement	x	y	z
OD	u	O	E	E	OX	u	O	O	O
	v	E	O	E		v	E	E	O
	w	E	E	O		w	E	O	E
EY	u	O	O	E	EZ	u	O	E	O
	v	E	E	E		v	E	O	O
	w	E	O	O		w	E	E	E
EX	u	E	E	E	EV	u	E	O	O
	v	O	O	E		v	O	E	O
	w	O	E	O		w	O	O	E
OY	u	E	E	O	OZ	u	E	O	E
	v	O	O	O		v	O	E	E
	w	O	E	E		w	O	O	O

the corresponding elements can be expressed in a fairly compact form. These are given in the Appendix.

The matrix equations are general and can accommodate approximating functions in (x,y) that are either global and analytic (such as Fourier or power series) or local and exactly evaluated (such as finite-element polynomials). The dependence on the z coordinate has been eliminated by preintegrating, which manifests itself in the matrix equations above. Because of the nature of the approximating functions themselves, the derivatives of the displacement are continuous over only a specific sublayer. If the material is homogeneous, this is still an acceptable approximation even for a subdivided layer because the behavior trends toward a continuous derivative as the number of layers increases. For the case of dissimilar media, the functions allow a break in the slope, which matches physical reality much more accurately than does a global approximation.

For a homogeneous isotropic parallelepiped, Ohno[3] showed that the eigenvalue problem in Eq. (8) can be split into eight smaller problems using symmetry arguments of the displacement-field components and matching these with the appropriate series terms in the approximation functions. These are denoted by the eight groups listed in Table I,[3] where the letters O and E, respectively, denote functions that are odd or even with respect to the appropriate spatial coordinate. For example, power series can be used for each of the displacement functions (such as in the powerful algorithm of Visscher and colleagues[7]). Including six terms in the Pascal-triangle visualization of the approximation functions (i.e., terms up to $x^5y^5z^5$) means a general eigenvalue problem for three unknowns with 6^3 terms in each, or an eigenvalue problem of dimension 648. If symmetry is used, this problem can be split into eight problems of dimension 81, greatly increasing the speed of this computation. This calculation must be completed many times when the elastic constants are being computed, and hence the splitting of the original problem possesses much appeal.

For the layered bimaterial, however, there is no material symmetry about the $x-y$ plane, and hence the splitting operation for this characteristic must be removed. This results not in eight groups, but four, which are the more generalized groups defined in Table I before exploiting symmetry about the $x-y$ plane. We define these four groups and their labeling in Table II.

TABLE II. Group structure for layered isotropic laminate.

Group	Displacement	x	y
1	u	E	E
	v	O	O
	w	O	E
2	u	E	O
	v	O	E
	w	O	O
3	u	O	O
	v	E	E
	w	E	O
4	u	O	E
	v	E	O
	w	E	E

IV. MEASUREMENTS

We measured three materials: nearly texture-free copper, 0.2W/Cu composite, and a three layer 0.2W/Cu–Cu-0.2W/Cu laminate. Using an optical microscope, we measured layer thicknesses of 0.150–0.188-0.166 cm for the laminate. Mass densities were determined using Archimedes' method with distilled water as a standard. The copper contained a significant volume fraction of voids that lowered the expected mass density by about 8%. The composite specimen contained about 1% voids. For the elastic-constants determination, we used URS as described in the previous section and by Migliori and Sarrao[6] for homogeneous materials.

The sending and receiving transducers were poled polycrystalline lead zirconate titanate (PZT) that hold the specimens by their corners diagonally. One transducer transmits continuous sinusoidal waves to the specimen, and the other transducer detects the specimen's displacement response.

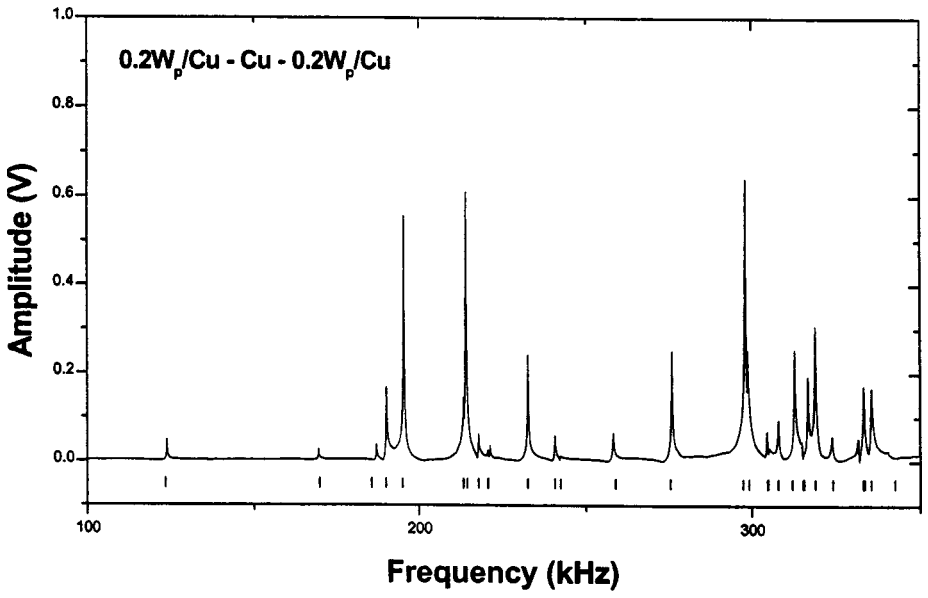

FIG. 2. Measured resonance spectrum of trilayer laminate. Resonant frequencies yield the C_{ij}. The bars at the bottom of the figure indicate resonance frequencies calculated from the deduced C_{ij}.

Their center frequencies were 10 MHz. Their broadband character permits using them far from their resonance frequencies, thus minimizing the piezoelectric-crystal contributions to the systems macroscopic frequencies and damping. Figure 2 shows the frequency-response spectrum for the layered composite. The two separate constituent materials also have a response spectrum, but their individual behavior is used only to compare with the results from our layered model, and hence these are not shown. As discussed above, the resonance frequencies depend on specimen shape, size, mass (or mass density), elastic stiffnesses, and layer thicknesses. Although not reported, internal frictions can be calculated from the half-power width of associated resonance peaks.

V. RESULTS AND DISCUSSION

The general procedure that forms the foundation of using URS to calculate the elastic constants is to iteratively select the elastic constants that give the best fit to the measured frequencies. This is accomplished by minimizing the differences between the measured and experimental frequencies using the Levenburg–Marquardt algorithm.[13] Details of this procedure are described by Migliori and Sarrao.[6]

Two types of models are used to determine the elastic constants of the constituent materials used in this study. The model of most interest is the discrete-layer model described above, which is necessary to represent the through-thickness behavior of the layered material. However, we also use a simpler method to calculate the elastic constants of each of the two constituent materials when these materials appear in a homogeneous block. In this case, global basis functions with C^1 continuity can be used since the displacement gradients are continuous within the deformed (vibrating) solid. Our weak form and matrix equations now remain the same, but in this case our z-direction approximations retain the form used for the in-plane approximation functions. This methodology is well developed (see, for example, Refs. 6 and 5) and we will not discuss it here other than to note that we used the same fitting procedure for the experimental frequencies of the homogeneous blocks as we did for the layered material, with a resulting frequency rms error of 0.11 percent for the Cu and 0.08 percent for the W_p/Cu composite. We note that for the homogeneous block, only two elastic parameters are fit to the measured frequencies; for the layered block, there are four.

It is usually necessary to use a number of frequencies at least five times larger than the number of unknown constants to be determined.[6] In this application, we use the lowest 29 frequencies in our inversion scheme for the layered material. Although it is not uncommon to have missing modes in a response spectrum, that is not the case here and our theoretical frequencies show a very strong relationship with the experimental frequencies. We iteratively solve the eigenvalue problem given in Eq. (8) until the differences between the measured and computed frequencies reach a minimum. The initial guess for the elastic constants has no effect on the final values provided they are within a reasonable range (5–10 percent) of the final elastic constants. This point is discussed in more detail by Migliori and Sarrao.[6]

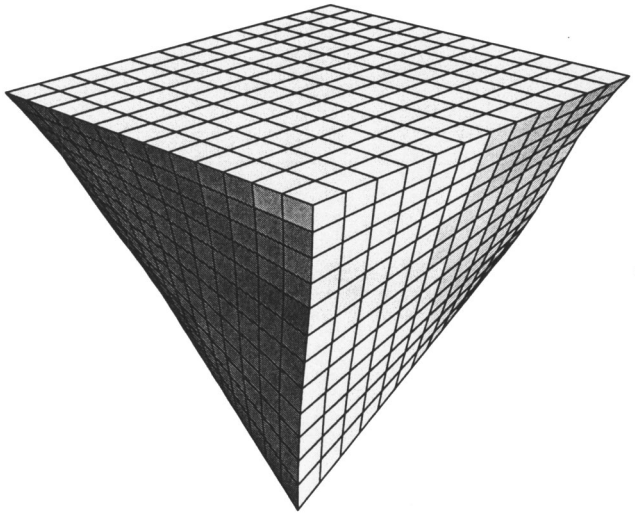

FIG. 3. Modal shape for the lowest mode in group 2 (and lowest overall frequency) for layered bimaterial. Physically, this corresponds to shear in the $x-y$ plane. This is the first nonzero frequency in group 2. This modal group has one rigid-body mode with zero frequency.

The 29 frequencies used in the minimization procedure can be split into four groups as described above. Each of these frequencies has a corresponding modal displacement pattern of the deformation pattern the specimen undergoes as it oscillates at this frequency. In Figs. 3–6 we show the lowest nonzero modal pattern for each of the four groups. For the type of assumed displacement field we have used in our solution methodology, there are six rigid-body modes (three translational and three rotational) that result in a displacement with zero strain energy. These each yield a frequency of 0, and are not included in our results other than to note that groups 1 and 3 possess one each of these modes, with groups 2 and 4 possessing two each. In several of these figures

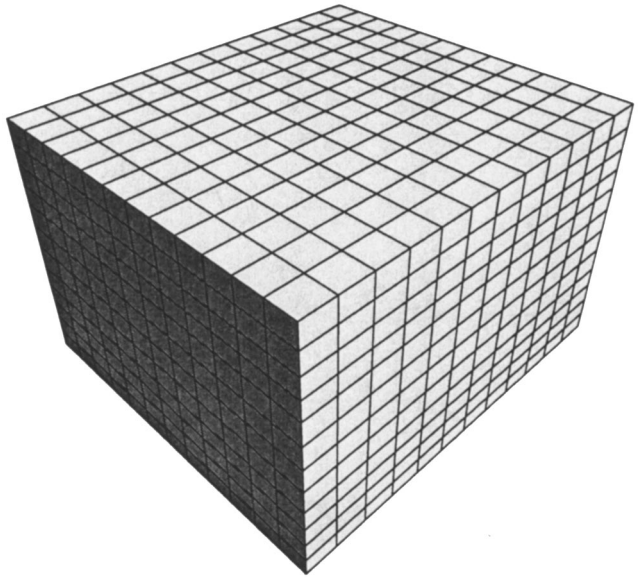

FIG. 4. Modal shape for the lowest mode in group 4 for layered bimaterial. This mode corresponds to the breathing mode associated with the flat faces remaining nearly plane but undergoing uniform deformation across each of the six faces. This is the first nonzero frequency in group 4 which, as in group 2, also has a single rigid-body mode.

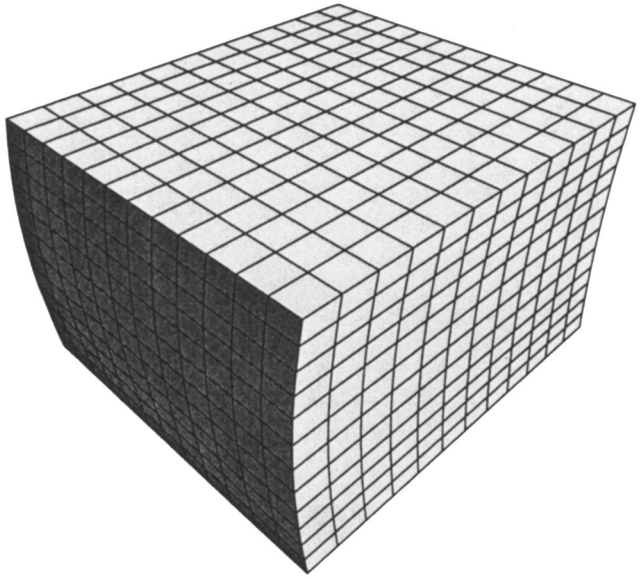

FIG. 5. Modal shape for the lowest mode in group 1 for layered bimaterial. This group has two rigid-body modes.

(where four divisions have been used for each physical layer of the specimen), the modal patterns show the break in the shear strain at a dissimilar material interface, indicating the need for appropriate approximating functions through the thickness.

The final values for the elastic constants of the two constituent materials are given in Table III, and were calculated with a final rms error in frequency of 0.26 percent. In this table, the elastic constants are compared with values calculated using methods described above. Our theoretical model for the layered material assumes that each of the layers is isotropic, and hence we estimate a single C_{11} and C_{44} for each of the two layers. The good fit to the measured frequencies is further demonstrated in Table IV, where we show the

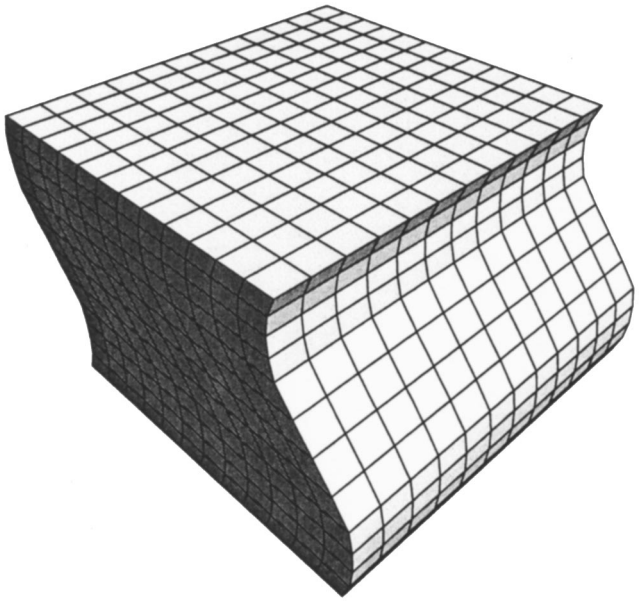

FIG. 6. Modal shape for the lowest mode in group 3, which also has two zero rigid-body frequencies and corresponding modal shapes.

TABLE III. Calculated material properties for Cu and 0.2 W_p/Cu composite. The subscript H denotes that a homogeneous specimen was used to calculate the elastic properties, whereas the subscript L denotes calculation using the layered specimen and discrete-layer theoretical model that is the primary focus of this study. The parameters C_L, B, G and E, are the longitudinal, bulk, shear, and Young moduli, and ν and c are the Poisson ratio and void volume fraction, respectively. All constants are in GPa except ρ, ν, and c.

	Cu (URS_H)	Cu (URS_L)	0.2 W_p/ Cu (URS_H)	0.2 W_p/ Cu (URS_L)
ρ (g/cm^3)	8.2348		10.8954	
C_{11}	155.71		239.74	
C_{22}	157.79	154.88	240.30	242.18
C_{33}	155.31		233.23	
C_{44}	40.001		60.015	
C_{55}	39.953	40.25	59.985	60.31
C_{66}	40.175		60.845	
C_{12}	76.518		118.51	
C_{13}	75.733	74.37	116.83	121.56
C_{23}	76.557		116.95	
C_L	156.30		237.80	
B	102.93		157.52	
G	40.025		60.213	
E	106.30		160.22	
ν	0.3279		0.3305	
c	0.078		0.009	

measured frequencies compared with the theoretical frequencies as calculated using the final elastic constants for the two layers. Also shown in this table are the frequencies that would result if the parallelepiped were a homogeneous block of either of the two materials, with block H1 denoting a homogeneous block of 20 percent tungsten and H2 a homogeneous block of pure copper. Lack of significant anisotropy in the elastic constants shown in Table IV reveals nearly texture-free materials, as expected for powder-metallurgy preparation.

Our results for C_{11} lie within 0.9% of those of the average equivalent moduli for the Cu and 1.9% of the W_p/Cu composite. Our values for C_{44} are within 0.6% and 0.05% for the same two materials, respectively. It is quite possible that for a block with such a low aspect ratio, modes involving shear deformation are more dominant, leading to better agreement for the shear moduli than that of C_{11}. Other natural sources of error include the precise nature of the dissimilar-layer bond and our treating each of the materials as isotropic in our layered model.

Our ability to extract the elastic constants of individual layers within a laminate could prove to be significant for certain types of materials for which a homogeneous specimen may be difficult to procure. Thin films on substrates or natural multilayered solids could potentially be studied using this approach without having to separate the materials for individual examination. Though not without limitations, we have shown for the first time that ultrasonic-resonance spectroscopy methods can be applied to layered systems with reasonably good results. Applications to more complex systems await future study.

TABLE IV. Modal groups and frequencies (in Hz) for laminated and homogeneous blocks.

Mode	ω_{exp}	ω_{lay}	G_{lay}	ω_{H1}	G_{H1}	ω_{H2}	G_{H2}
1	123 942	123 427	2	129 045	2	105 420	2
2	169 557	169 834	4	175 576	4	143 242	4
3	187 150	185 726	2	203 567	1	165 928	1
4	190 199	189 992	1	207 530	2	169 501	2
5	195 462	195 012	2	211 099	2	172 448	2
6	213 480	213 429	3	225 387	4	183 066	4
7	214 272	214 545	4	232 775	4	190 131	4
8	218 005	217 919	4	237 165	1	193 545	1
9	220 732	220 782	1	237 460	3	193 662	3
10	221 446	220 885	3	238 123	3	194 436	3
11	232 966	232 829	1	258 947	3	211 037	3
12	241 005	240 977	4	260 030	1	212 193	1
13	242 515	242 622	3	262 221	4	213 874	4
14	258 394	259 043	4	287 736	4	234 620	4
15	276 146	275 605	1	297 445	1	242 835	1
16	298 201	297 474	2	323 122	1	263 872	1
17	298 964	299 177	1	324 685	3	265 165	3
18	304 732	304 759	3	326 833	3	266 848	3
19	305 277	305 047	3	327 795	2	267 450	2
20	308 197	308 117	2	330 751	4	269 744	4
21	313 024	312 235	4	350 621	1	285 526	1
22	315 030	315 415	3	351 051	3	285 749	4
23	316 972	315 811	4	351 535	4	285 912	3
24	319 186	319 121	1	351 595	2	286 695	2
25	324 133	324 330	4	359 377	4	292 252	4
26	331 772	333 170	1	363 043	4	296 226	4
27	333 451	333 674	4	370 136	2	302 195	2
28	335 782	335 629	3	372 100	4	303 725	4
29	340 605	342 694	4	381 167	1	310 452	1

VI. CONCLUSIONS

(1) Discrete-layer models that account for kinks in displacement gradients across a dissimilar-material interface are crucial in obtaining accurate theoretical frequency predictions and subsequent estimates of elastic constants.
(2) Ultrasonic-resonance spectroscopy can be applied to layered isotropic laminates with good accuracy. For a trilayer composite, we found matching of the first 29 frequencies yielding an rms error of 0.26 percent between theoretical and measured frequencies. There were no missing modes.
(3) Layer elastic constants of the two dissimilar materials agree with elastic constants computed using homogeneous specimens within 0.9 percent for the Cu and 1.9 percent for the W_p/Cu composite for C_{11}, and within 0.6 and 0.05 percent, respectively, for C_{44}.

ACKNOWLEDGMENTS

P.R.H. acknowledges support of the Alexander von Humboldt Research Foundation in Germany. I.R. acknowledges support from the U.S. Army Research Office, Grant No. DAAD19-01-1-0590.

APPENDIX:

The entries in the element coefficient matrices can be expressed as

$$[K^{11}]_{\alpha\beta}=\int_A\left[[A^{11}]\frac{\partial\Psi^u_\alpha}{\partial x}\frac{\partial\Psi^u_\beta}{\partial x}+[D^{55}]\Psi^u_\alpha\Psi^u_\beta+[A^{66}]\frac{\partial\Psi^u_\alpha}{\partial y}\frac{\partial\Psi^u_\beta}{\partial y}\right]dx\,dy, \tag{A1}$$

$$[K^{12}]_{\alpha\beta}=\int_A\left[[A^{12}]\frac{\partial\Psi^u_\alpha}{\partial x}\frac{\partial\Psi^v_\beta}{\partial y}+[A^{66}]\frac{\partial\Psi^u_\alpha}{\partial y}\frac{\partial\Psi^v_\beta}{\partial x}\right]dx\,dy, \tag{A2}$$

$$[K^{13}]_{\alpha\beta}=\int_A\left[[B^{13}]\frac{\partial\Psi^u_\alpha}{\partial x}\Psi^w_\beta+[\bar{B}^{55}]\Psi^u_\alpha\frac{\partial\Psi^w_\alpha}{\partial x}\right]dx\,dy, \tag{A3}$$

$$[K^{22}]_{\alpha\beta}=\int_A\left[[A^{22}]\frac{\partial\Psi^v_\alpha}{\partial y}\frac{\partial\Psi^v_\beta}{\partial y}+[D^{44}]\Psi^v_\alpha\Psi^v_\beta+[B^{24}]^T\Psi^v_\alpha\frac{\partial\Psi^v_\beta}{\partial y}+[A^{66}]\frac{\partial\Psi^v_\alpha}{\partial x}\frac{\partial\Psi^v_\beta}{\partial x}\right]dx\,dy, \tag{A4}$$

$$[K^{23}]_{\alpha\beta}=\int_A\left[[B^{23}]\frac{\partial\Psi^v_\alpha}{\partial y}\Psi^w_\beta+[\bar{B}^{44}]\Psi^v_\alpha\frac{\partial\Psi^w_\alpha}{\partial y}\right]dx\,dy, \tag{A5}$$

$$[K^{33}]_{\alpha\beta} = \int_A \left[[A^{44}] \frac{\partial \Psi_\alpha^w}{\partial y} \frac{\partial \Psi_\beta^w}{\partial y} + [D^{33}] \Psi_\alpha^w \Psi_\beta^w + [A^{55}] \frac{\partial \Psi_\alpha^w}{\partial x} \frac{\partial \Psi_\beta^w}{\partial x} \right] dx\, dy. \tag{A6}$$

The submatrices listed above are computed by preintegrating the functions in z. For any general approximation through the thickness, these can be expressed as

$$A_{ij}^{km} = \sum_{l=1}^{N} \int_{z_l}^{z_{l+1}} C_{km} \bar{\Psi}_i(z) \bar{\Psi}_j(z) dz, \tag{A7}$$

$$B_{ij}^{km} = \sum_{l=1}^{N} \int_{z_l}^{z_{l+1}} C_{km} \bar{\Psi}_i(z) \frac{d\bar{\Psi}_j(z)}{dz} dz, \tag{A8}$$

$$\bar{B}_{ij}^{km} = \sum_{l=1}^{N} \int_{z_l}^{z_{l+1}} C_{km} \bar{\Psi}_i(z) \bar{\Psi}_j(z) dz, \tag{A9}$$

$$D_{ij}^{km} = \sum_{l=1}^{N} \int_{z_l}^{z_{l+1}} C_{km} \frac{d\bar{\Psi}_i(z)}{dz} \frac{d\bar{\Psi}_j(z)}{dz} dz. \tag{A10}$$

[1] E. P. Eer Nisse, "Variational method for electroelastic vibration analysis," IEEE Trans. Sonics Ultrason. **SU-14**, 153–160 (1967).

[2] H. H. Demarest, Jr., "Cube resonance method to determine the elastic constants of solids," J. Acoust. Soc. Am. **49**, 768–775 (1971).

[3] I. Ohno, "Free vibration of a rectangular parallelepiped crystal and its application to determination of elastic constants of orthorhombic crystals," J. Phys. Earth **24**, 355–379 (1976).

[4] P. R. Heyliger, A. Jilani, H. Ledbetter, R. Leisure, and C.-K. Wang, "Elastic constants of isotropic cylinders using resonant ultrasound," J. Acoust. Soc. Am. **94**, 1482–1487 (1995).

[5] H. Ledbetter, C. Fortunko, and P. Heyliger, "Orthotropic elastic constants of a boron–aluminum fiber-reinforced composite: An acoustic-resonance-spectroscopy study," J. Appl. Phys. **78**, 1542–1546 (1995).

[6] A. Migliori and J. L. Sarrao, *Resonant Ultrasound Spectroscopy: Applications to Physics, Materials Measurements and Non-Destructive Evaluation* (Wiley, New York, 1997).

[7] W. M. Visscher, A. Migliori, T. M. Bell, and R. A. Reinert, "On the normal modes of free vibration of inhomogeneous and anisotropic elastic objects," J. Acoust. Soc. Am. **90**, 2154–2162 (1991).

[8] P. Heyliger, "Traction-free vibration of layered elastic and piezoelectric parallelepipeds," J. Acoust. Soc. Am. **107**, 1235–1245 (2000).

[9] K. E. Pauley and S. B. and Dong, "Analysis of Plane Waves in Laminated Piezoelectric Plates," Wave Electron. **1**, 265–285 (1976).

[10] J. N. Reddy, "A generalization of displacement-based laminate theories," Commun. Appl. Numer. Methods **3**, 173–181 (1987).

[11] Atlantic Equipment Engineering, Bergenfield, NJ. Products or companies named here are cited only in the interest of complete scientific description, and neither constitute nor imply endorsement by NIST or by the US government. Other products may be found to serve just as well.

[12] Goodfellow Cambridge Ltd., Huntington, England.

[13] W. H. Press, B. P. Flannery, S. A. Teukolsky, and W. T. Vetterling, *Numerical Recipes* (Cambridge University Press, Cambridge, 1986), Chap. 15.

[14] H. F. Tiersten, *Linear Piezoelectric Plate Vibrations* (Plenum, New York, 1969).